

## Article

# Identification of Novel Potential Heparanase Inhibitors Using Virtual Screening

Alfredo Rus<sup>1</sup>, Victor M. Bolanos-Garcia<sup>2</sup> , Agatha Bastida<sup>1,\*</sup>  and Paula Morales<sup>3,\*</sup> 

<sup>1</sup> Departamento de Química Bio-Orgánica, Instituto de Química Orgánica General (IQOG-CSIC), CSIC, c/Juan de la Cierva 3, 28006 Madrid, Spain; alrus@ucm.es

<sup>2</sup> Department of Biological and Medical Sciences, Faculty of Health and Life Sciences, Oxford Brookes University, Oxford OX3 0BP, UK; vbolanos-garcia@brookes.ac.uk

<sup>3</sup> Instituto de Química Médica (IQM-CSIC), Juan de la Cierva 3, 28006 Madrid, Spain

\* Correspondence: agatha.bastida@csic.es (A.B.); paula.morales@iqm.csic.es (P.M.)

**Abstract:** Heparanase (HPSE) is a mammalian endo- $\beta$ -D-glucuronidase that cleaves heparan sulphate (HS) side chains of heparin sulphate proteoglycans (HSPG), a class of molecules composed of repeating polysulfated disaccharide units of glucosamine and hexuronic acid residues. HPSE controls the availability of growth factors, chemokines, lipoproteins and other bioactive molecules by degrading HS into smaller fractions, allowing the release of saccharide fragments that activate a plethora of signaling processes. HPSE overexpression has been correlated with tumor survival and metastasis as well as several diseases associated with chronic inflammation, including the ongoing COVID-19 pandemic caused by SARS-CoV-2. Thus, the search for molecules that could potentially inhibit HPSE has become increasingly relevant in the clinic. In this study, we have integrated a strategy that combines virtual screening and molecular docking of publicly available chemical databases to identify small compounds that can be developed into novel HPSE inhibitors. Structural rationalization of the interactions previously reported compounds led us to identify promising unexplored chemotypes. Here we show that these novel potential HPSE inhibitors present optimized in silico druggability and docking properties and may serve as pharmacological tools for the treatment of chronic and infectious diseases associated with chronic inflammation.

**Keywords:** COVID-19; docking; heparanase (HPSE); inhibitors; virtual screening



**Citation:** Rus, A.; Bolanos-Garcia, V.M.; Bastida, A.; Morales, P. Identification of Novel Potential Heparanase Inhibitors Using Virtual Screening. *Catalysts* **2022**, *12*, 503. <https://doi.org/10.3390/catal12050503>

Academic Editor: Rong Shi

Received: 18 March 2022

Accepted: 28 April 2022

Published: 30 April 2022

**Publisher's Note:** MDPI stays neutral with regard to jurisdictional claims in published maps and institutional affiliations.



**Copyright:** © 2022 by the authors. Licensee MDPI, Basel, Switzerland. This article is an open access article distributed under the terms and conditions of the Creative Commons Attribution (CC BY) license (<https://creativecommons.org/licenses/by/4.0/>).

## 1. Introduction

Heparanase (HPSE) is an enzyme that plays a key role in the control of the availability of growth factors, chemokines, lipoproteins and other bioactive molecules that bind heparan sulphate (HS), an interaction that is critical for the modulation of numerous signaling pathways [1,2]. Under specific physiopathological circumstances, HPSE overexpression correlates with tumor survival and metastasis as well as several diseases associated with chronic inflammation. More recently, overexpression of HPSE has been observed in severe acute respiratory syndrome coronavirus 2 (SARS-CoV-2) infections [1]. Thus, the identification of potential inhibitors of this target is a very promising therapeutic approach to treat COVID-19 and other chronic inflammation associated diseases.

As proven by the crystal structure of HPSE [3], the active enzyme is a non-covalently linked heterodimer consisting of an 8 kDa N-terminal and a 50 kDa C-terminal polypeptide chains. Site-directed mutagenesis has confirmed the presence of two catalytic residues that act as proton donor (Glu225) and nucleophile (Glu343), respectively. The crystal structure of HPSE also revealed two catalytic residues that are located in a cleft of  $\sim 10$  Å length within the  $(\beta/\alpha)_8$  domain and lined with the basic side chains of arginine and lysine residues. Both sides of this  $(\beta/\alpha)_8$  domain are flanked by a small sandwich domain. One  $\beta$ -sheet of the  $\beta$ -sandwich as well as the first  $\beta$ - $\alpha$ - $\beta$  fold of the  $(\beta/\alpha)_8$  domain is provided by the small 8 kDa chain (Figure 1) [3,4]. HPSE favors the cleavage of the bond of a glucuronic

acid linked to 6-O-sulfated glucosamine that may be *N*-sulfated or *N*-acetylated and as a strict *endo*- $\beta$ -D-glucuronidase, it can only cleave internal linkages [4–6]. As depicted in Figure 1, the binding site is surrounded by two heparin binding domains HBD-1 and HBD-2 which are two short amino acid sequences rich in arginine and lysine residues [7]. Close to the catalytic residues, a glycine loop acts as the recognition site for the carboxylate group of the substrate glucuronic acid (Figure 1).

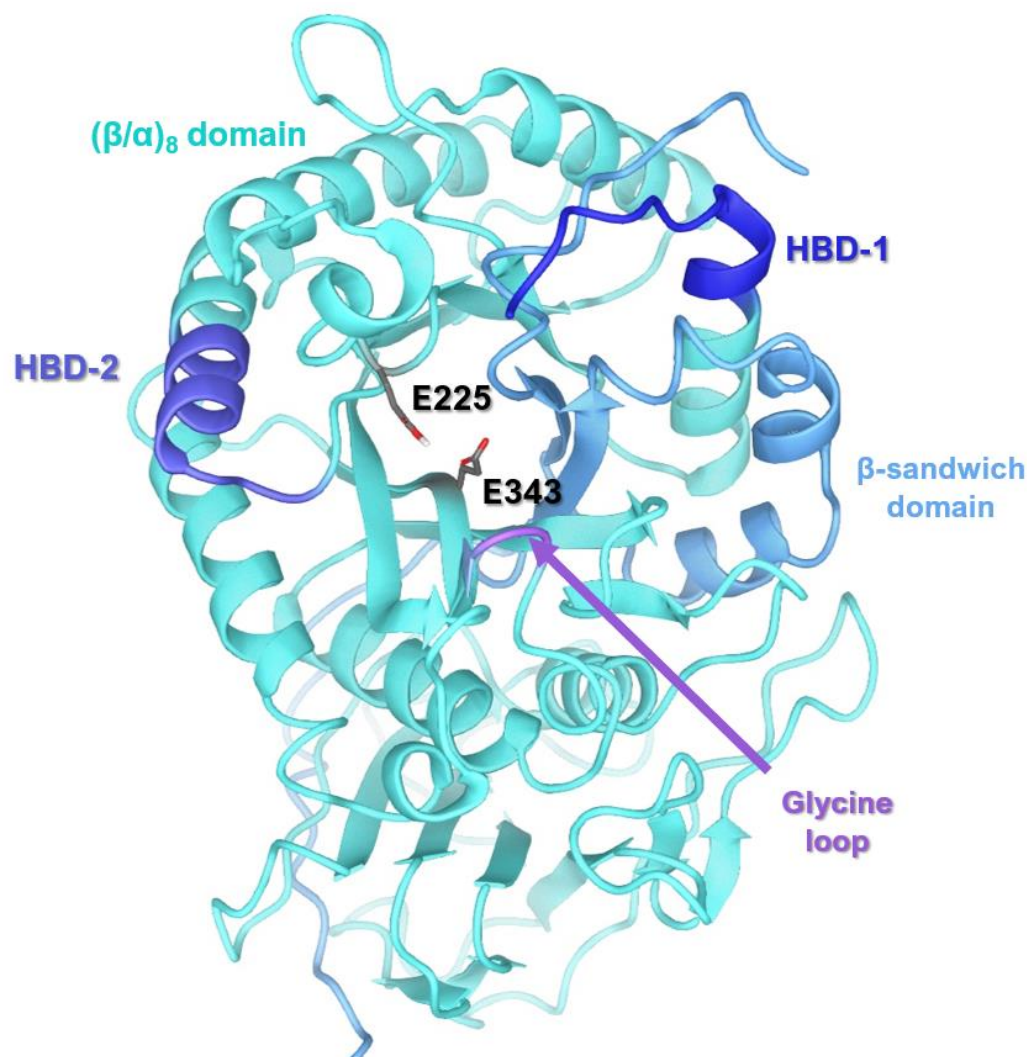


**Figure 1.** Three-dimensional structure of human heparanase, HPSE (PDB ID:5E9C). Chain-A, the  $(\beta/\alpha)_8$  domain, is shown in cyan, and chain-B, the  $\beta$ -sandwich containing domain, in light blue. The heparin binding domain 1 (HBD-1) is depicted in dark blue, and the heparin binding domain 2 (HBD-2) in light purple. The glycine loop is highlighted in magenta and the catalytic residues in grey.

Due to the implication of HPSE in malignancies associated with chronic inflammation, diverse approaches have been proposed to inhibit HPSE activity. The first strategies were based on chemical modifications of its natural substrates (heparins or sulfated oligosaccharides), such as the case of muparfostat [8,9], necuparanib [10–12] and roneparstat [13–18], or synthetic compounds such as pixatimod [19–22] (Figure S1), which are, as of today, the only HPSE inhibitors that have reached the clinical trials stage. Furthermore, a compound consisting of 12 repeating units of GlcNS(6S) $\alpha$ (1,4)GlcA (Figure S1) appeared to be one of the most potent HPSE inhibitors reported to date [23]. Other potent inhibitors have emerged from polysaccharides [5,23], their high molecular weight and heterogeneity importantly affects their potential use as *bona fide* drugs [24].

Although a few small size natural products arise as potential HPSE inhibitors such as (+)-trachyspic acid, a metabolite produced by *Talaromyces trachyspermus* SANK [25], certain fungal metabolites from *Acremonium* sp. [26], berberine, a natural isoquinoline alkaloid [27], the natural sesquiterpene  $\beta$ -elemene [28] and  $\lambda$ -carrageenan extracted from red seaweed [29,30] (Figure S1), it is due to drug discovery projects that synthetic small molecules with great potential to inhibit HPSE have been developed (Figure 2) [24,31]. Indeed, some of these small size compounds have reached preclinical stages. For instance, the urea-based low-molecular-weight compound suramin (Figure S1) and its derivatives, have been reported as non-competitive inhibitors of HPSE [32]. Another group of HPSE inhibitors are based on the benzazoly scaffold, including benzimidazole, benzoxazole and benzothiazole derivatives (Figure S1) [33] and on furanyl-1,3-thiazole-2-yl-acetic acid derivatives (Figure S1) [34]. More recently, an in vitro screening identified [1,2,4]triazolo [3,4-*b*] [1,3,4]thiadiazole derivatives as active substances against HPSE (Figure S1) [35]. Interestingly, virtual screening of a commercial collection of drug-like compounds led to the identification of the antimalarial drug amodiaquine (Figure S1), which acts as a HPSE inhibitor with micromolar affinity [36].

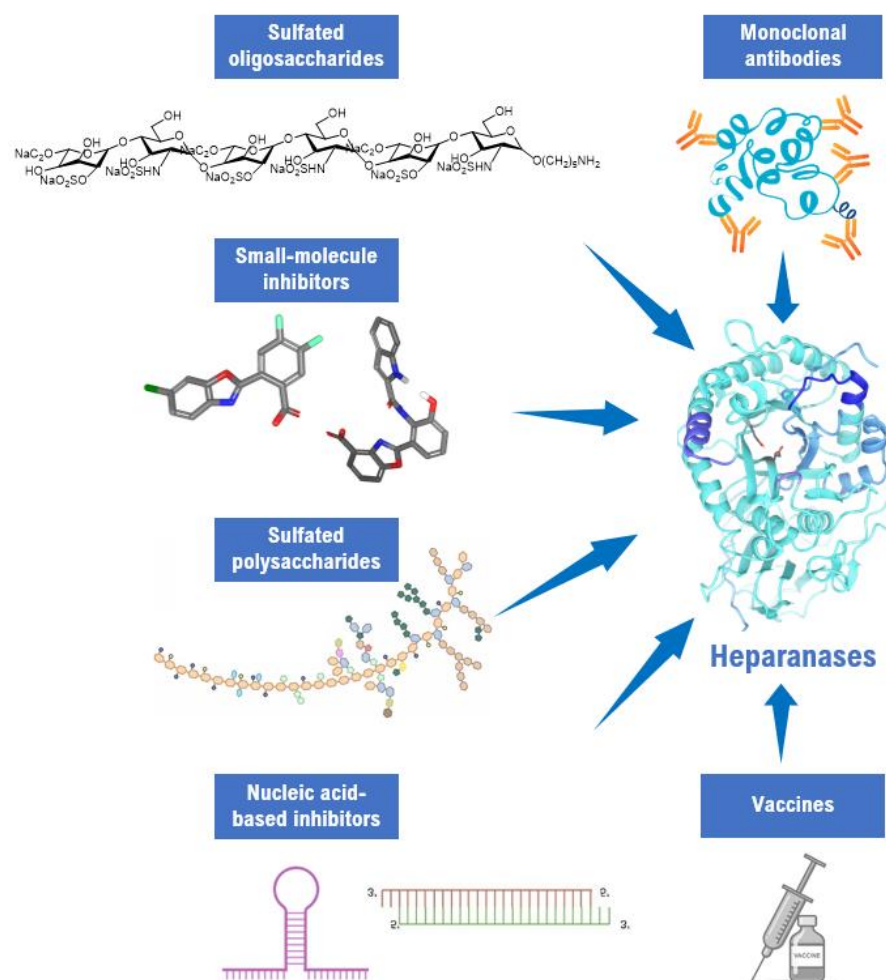


**Figure 2.** Approaches developed to suppress *hpse* gene expression and inhibit HPSE catalytic activity [37].

The 3D structural information of the protein that is currently available is of paramount importance to facilitate the rational design of more effective HPSE inhibitors. In this study, we report the identification of potential new HPSE inhibitors using a strategy that integrated the virtual screening of over 80,000 small size chemical compounds deposited in open access databases with molecular docking approaches. Taking into account chemical

structure diversity, reported HPSE inhibitory activity and mode of binding to the protein target HPSE, promising hit compounds were selected. Further investigations will aim to develop them into a series of lead compounds, with the ultimate goal of developing new inhibitors for the treatment of diseases associated with chronic inflammation.

## 2. Results and Discussion

The in silico identification of potential HPSE inhibitors has been pursued following the workflow detailed in Figure S2.

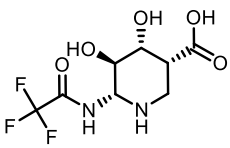
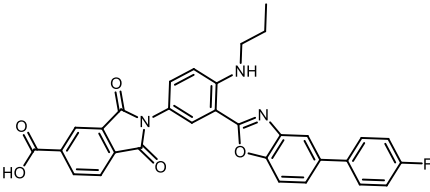
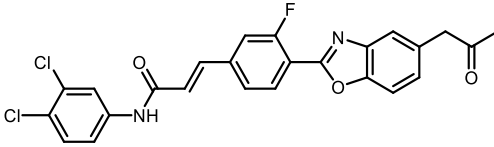
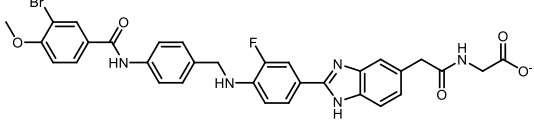
### 2.1. Structural Evaluation of Reported Inhibitors

We first aimed to rationalize key structural features leading to the inhibition of heparanase catalytic activity. For this, we retrieved reported HPSE inhibitors from the ChEMBL database [38,39]. A total of 573 known ligands of human HPSE were analyzed using the DataWarrior software. Upon duplicate removal and filtering-off compounds with no relevant inhibitory capacity, we performed docking studies with the 282 most relevant HPSE inhibitors reported to date.

For this purpose, extra-precision (XP) Glide molecular docking, as implemented in the Maestro software (Schrödinger, LLC, New York, United States), was performed using the HPSE crystal structure solved at 1.73 Å resolution (PDB-ID: 5E9C) [24]. Protein optimization and ligand conformational analyses were carried out prior to the docking of the aforementioned 282 known HPSE inhibitors (see Section 3 and Table S1).

The docking scores and specific mode of binding to the HPSE residues defining the catalytic pocket were analyzed and compared with their reported IC<sub>50</sub> values (Table S2—Supplementary Material spreadsheet). In addition to this analysis, we took into account chemical diversity, lack of reported off-target effects and general occupancy of the binding crevice as selection criteria to select the best compounds for further chemoinformatics studies. This manner, the compounds ChEMBL2349245, ChEMBL495255, ChEMBL2349247 and ChEMBL4294823 (Table 1) were selected and analyzed as shown below.

**Table 1.** Structure, IC<sub>50</sub> and docking scores of the selected HPSE inhibitors ChEMBL2349245, ChEMBL495255, ChEMBL2349247 and ChEMBL4294823.

Compound ID	Structure	Glide Score (kcal/mol)	IC <sub>50</sub> (μM)	References
ChEMBL2349245		−7.86	1	[40]
ChEMBL495255		−5.79	0.50	[36]
ChEMBL2349247		−5.60	0.20	[36]
ChEMBL4294823		−7.91	0.64	[41]



As depicted in Figure 3, compounds ChEMBL495255, ChEMBL2349247 and ChEMBL4294823 display an extended conformation within the HPSE pocket involving residues that form part of HBD-1, HBD-2 or both domains. In contrast, compound ChEMBL2349245, which is smaller and less flexible than ChEMBL495255, ChEMBL2349247 and ChEMBL4294823, is positioned in the middle of the binding site interacting with key catalytic residues (Glu225 and Glu343) and the glycine loop.

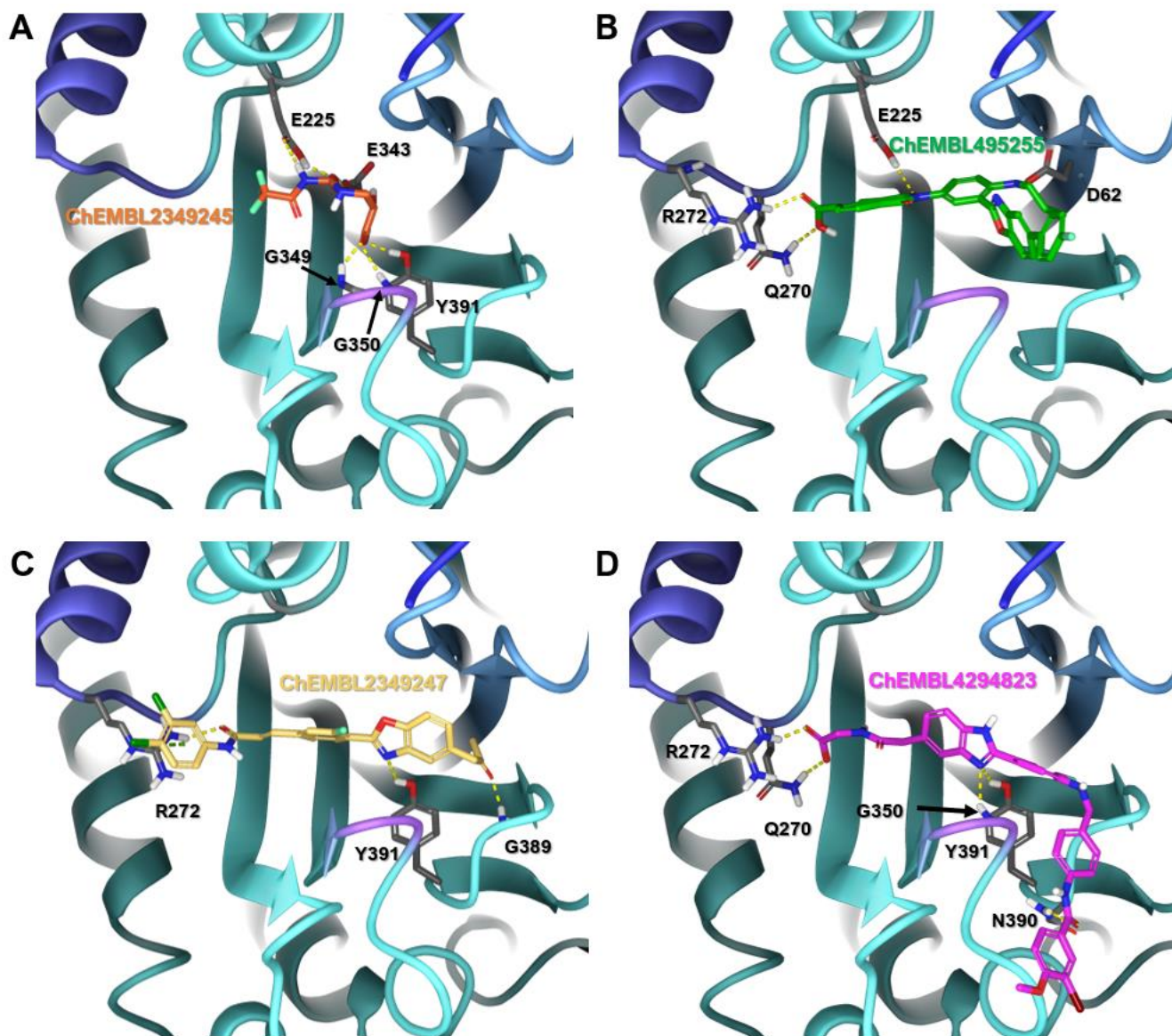


**Figure 3.** HPSE in complex with the selected reference hit compounds: (A) ChEMBL2349245 (orange); (B) ChEMBL495255 (green); (C) ChEMBL2349247 (ochre); (D) ChEMBL4294823 (pink tubes). H-bonds are shown in yellow dashed lines and pi-cation interactions in green. Molecules are shown in stick representation.

Figure 3 shows structural details of HPSE in complex with selected inhibitors. The smallest molecule, ChEMBL2349245, sits in the middle of the binding site, establishing H-bonding with both catalytic residues, Glu225 and Glu343. The HPSE-ChEMBL2349245 complex is further stabilized by the interaction of the ChEMBL2349245 acidic group with the HPSE glycine loop residues, Gly349 and Gly350, and with Tyr391, a residue involved in substrate recognition [37] (Figure 3A). The compound ChEMBL495255, on the other hand, extends in the crevice interacting with residues Gln270 and Arg272 of the HBD-2 (the

protein's main anchoring point [37]), and Asp62, a residue that is in close proximity to HBD-1 (Figure 3B). The compound ChEMBL495255 also establishes a H-bond interaction with the catalytic residue Glu225, further stabilizing the complex. In the HPSE-ChEMBL2349247 complex (Figure 3C), the 3,4-dichlorophenylamide group forms a H-bond and a pi-cation interaction with Arg272, a residue located within HBD-2. Moreover, the benzoxazol nitrogen forms a H-bond with Tyr391 while the backbone of Gly389, close to the HBD-1, establishes a H-bond with the carboxylic oxygen of the propanone benzoxazol substituent. ChEMBL4294823, the most extended compound of our list, interacts with residues Asn390 and Tyr391, Gly350 of the glycine loop, as well as residues Gln270 and Arg272 (Figure 3D). Ligand interaction diagrams are displayed in Figure S3.

Differences in the interacting patterns within the crevice, docking scores and the reported IC<sub>50</sub>s led us to select these molecules as chemical scaffolds for the ulterior search and development of novel, more potent HPSE inhibitors.

## 2.2. Virtual Screening of Structurally Related Chemical Databases

In order to identify new potential HPSE inhibitors, chemical libraries of compounds that are structurally related to the previously selected molecules (ChEMBL2349247, ChEMBL495255, ChEMBL4294823 and ChEMBL2349245) were carefully screened and analyzed.

Each of the hits thus identified was used as a molecular basis to retrieve four independent chemical libraries of compounds from PubChem with >0.7 or 0.8 Tanimoto similarity index (see Section 3) [42].

Upon data curation and conformational analyses, the structures contained within each library were screened using the Virtual Screening Workflow implemented in the Maestro software. Firstly, all the compounds were subjected to the High-Throughput Virtual Screening (HTVS) Glide docking protocol. Top-ranked ligands were then subjected to an extra precise (XP) Glide-dock screening. Docking glide scores, specific interactions with catalytic residues and structural diversity were considered for selecting the most promising inhibitors (Table 2).

To further filter off candidates, additional criteria such as ADME properties and the potential presence of structural promiscuous moieties or PAINS (pan-assay interference compounds) [43] were investigated for each molecule. For this purpose, a set of 34 chemical descriptors were calculated using the QikProp module integrated in the Maestro software. Structural alerts for each chemotype were identified using the swissADME webserver (Table 3).

**Table 2.** Selected compounds computed with their respective Glide docking score and reported IC<sub>50</sub> values.

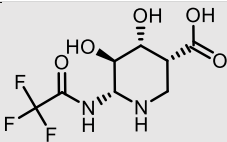
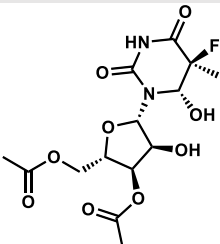
Compound ID	Structure	Glide Score (kcal/mol)	HPSE IC <sub>50</sub> (μM)	References
ChEMBL2349245		-7.86	1.00	[40]
101687126		-10.80	NR	[44]

Table 2. Cont.

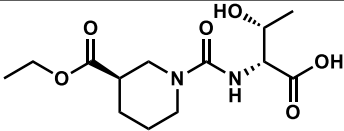
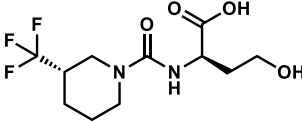
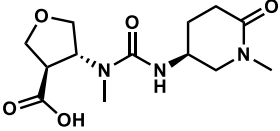
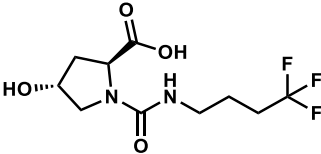
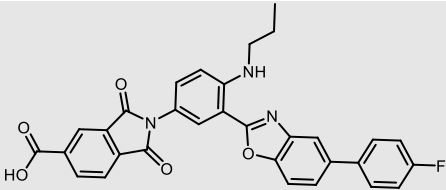
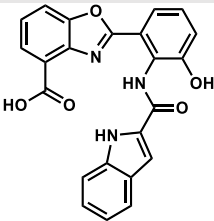
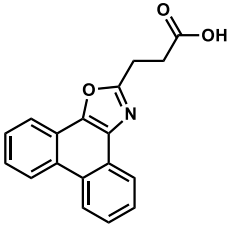
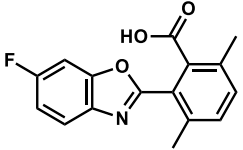
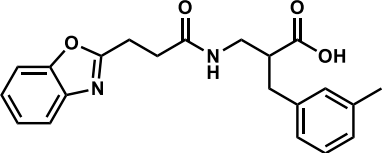
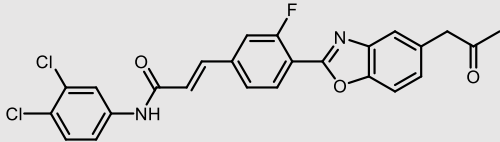
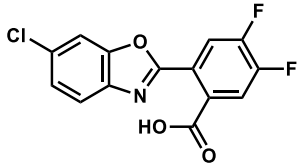
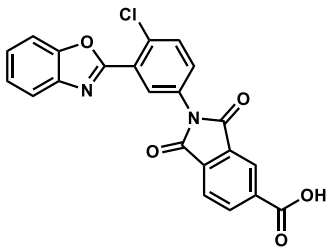
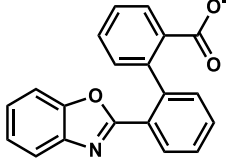
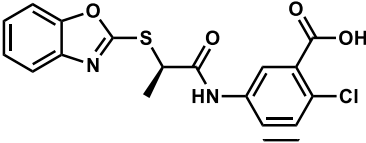
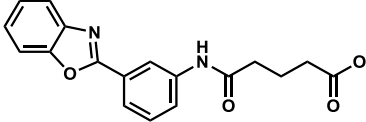
Compound ID	Structure	Glide Score (kcal/mol)	HPSE IC <sub>50</sub> (μM)	References
61187649		-9.53	NR	[45]
107828179		-9.04	NR	[46]
66265156		-8.88	NR	[47]
113327907		-8.54	NR	[47]
ChEMBL495255		-5.79	0.50	[36]
25158919		-9.33	NR	[48]
23794729		-8.31	NR	[49]
103430682		-8.01	NR	[50]
119243009		-7.44	NR	[51]

Table 2. Cont.

Compound ID	Structure	Glide Score (kcal/mol)	HPSE IC <sub>50</sub> (μM)	References
ChEMBL2349247		−5.60	0.20	[36]
81421830		−7.90	NR	[52]
58743027		−7.46	NR	[53]
155906206		−7.15	NR	[54]
23886486		−6.81	NR	[55]
6968873		−6.62	NR	[56]

NR: not reported.

Any compound exhibiting any violation of the Lipinski rules, PAINS alert, a Glide score above that of its reference compound, as well as any compound with a scaffold too similar to another within the same list or that was already reported to have anti-heparanase activity (Table S3), was excluded from the selection process.

Based on the aforementioned selection criteria, 14 compounds were identified as the most promising drug candidates (Table 2). As shown in this table, similarity-based chemical library screenings led to the selection of five compounds from the ChEMBL2349245 database; five from the ChEMBL2349247 database and four compounds from ChEMBL495255. Compounds drawn from the ChEMBL4294823 chemical library were discarded due to poorer docking values.

Importantly, the selected potential HPSE inhibitors not only exhibited a strong interaction pattern and docking scores but also a predicted a good druggability profile when compared to their reference compounds (Table 3).



**Table 3.** Physicochemical descriptors of selected compounds computed with QikProp and structural alerts (PAINS).

Compound	QPlogS <sup>a</sup>	QPlogHERG <sup>b</sup>	QPPCaco <sup>c</sup>	QPlogBB <sup>d</sup>	% Human Oral Absorption <sup>e</sup>	PAINS #
ChEMBL2349245	−0.72	−0.97	1.90	−1.00	15	0
101687126	−2.53	−3.81	78.62	−1.66	44	0
61187649	−2.77	−0.67	57.15	−1.23	69	0
107828179	−2.83	−0.64	30.74	−1.11	63	0
66265156	−0.50	1.22	30.14	−0.89	52	0
113327907	−2.13	−0.47	36.73	−0.93	62	0
ChEMBL495255	−8.64	−6.24	23.02	−2.27	58	0
25158919	−4.68	−4.76	66.73	−1.28	78	0
23794729	−4.34	−3.94	169.97	−0.78	87	0
103430682	−4.39	−3.21	411.40	−0.13	94	0
119243009	−4.82	−3.64	80.58	−1.38	84	0
ChEMBL2349247	−8.32	−7.43	818.21	−0.75	100	0
81421830	−4.63	−3.34	290.83	0.02	92	0
58743027	−6.07	−4.95	27.71	−1.51	73	0
155906206	−4.35	−4.08	387.64	−0.38	100	0
23886486	−4.35	−3.09	145.77	−0.66	85	0
6968873	−4.72	−4.77	58.63	−1.57	75	0

<sup>a</sup> Predicted aqueous solubility [−6.5/0.5]; <sup>b</sup> HERG K<sup>+</sup> Channel Blockage (log IC<sub>50</sub>) [concern below −5]; <sup>c</sup> Apparent Caco-2 cell permeability in nm/s [<25 poor, >500 excellent]; <sup>d</sup> Predicted log of the brain/blood partition coefficient [−3.0/1.2]; <sup>e</sup> Human Oral Absorption in GI [<25% is poor] [range of 95% of drugs]. # Number of structural alerts as calculated using the swissADME webservice [43].

The interaction of potential HPSE inhibitors that exhibited a promising profile (e.g., the best hits from each chemical library: 101687126, 25158919 and 81421830) are shown in Figure 4. A more extended list of the top hits (e.g., compounds 61187649, 107828179, 66265156, 113327907, 23794729, 103430682, 119243009, 58743027, 155906206, 23886486 and 6968873) is shown in Figure S4. Two-dimensional diagrams of the HPSE–inhibitor interactions are depicted in Figure S5.

Compounds derived from the ChEMBL2349245 library exhibited most of the desired interactions for a potential HPSE inhibitor. Namely, H-bonds with the catalytic residues Glu225 and Glu343, as well as Gln270 and Arg272, thus ensuring the anchoring of the molecule to HBD-2. The compounds derived from ChEMBL2349245 also establish H-bonds with residues from the HBD-1, either Asp62 or Thr97, Gly349, Gly350 (glycine loop), Tyr298 and Tyr391. The most remarkable small molecule from this subset is 101687126, which not only showed better interaction energy and network of interactions (Figure 4A) than the reference compound ChEMBL2349245, but also a predicted better absorption and cell permeability.

The best compounds retrieved from the ChEMBL495255 chemical library were smaller and more centered into the catalytic region than their reference compound. Although they lack direct interactions with residues from the HBD-2, this seems to be greatly compensated by establishing very favorable interactions with the glycine loop, catalytic residues and Tyr298 and Tyr391, and polar and charged aminoacids Lys232 and Ser228. All the selected molecules from this library greatly improved the aqueous solubility and cardiotoxicity predictions when compared to their reference hit ChEMBL495255 (Table 3). Figure 4B shows the docking of compound 25158919, the most remarkable molecule from this subset, to HPSE.

The compounds selected from the ChEMBL2349247 chemical library showed a wider variety of interactions with HPSE. While the compounds all preserved interactions with the catalytic Glu225, the glycine loop and Tyr391, some of them extended through the whole pocket while others only established interactions with HBD-1 or HBD-2 (Figures 4C and S4). Compound 81421830 presents the best docking values as well as predicted ADME profile. As shown in Figure 4C, in addition to the previously mentioned H-bonds with Glu255,

Tyr391, Gly349 and Gly350, it establishes halogen bond interactions with Arg272 and Gln270 and pi-stackings with Tyr298.

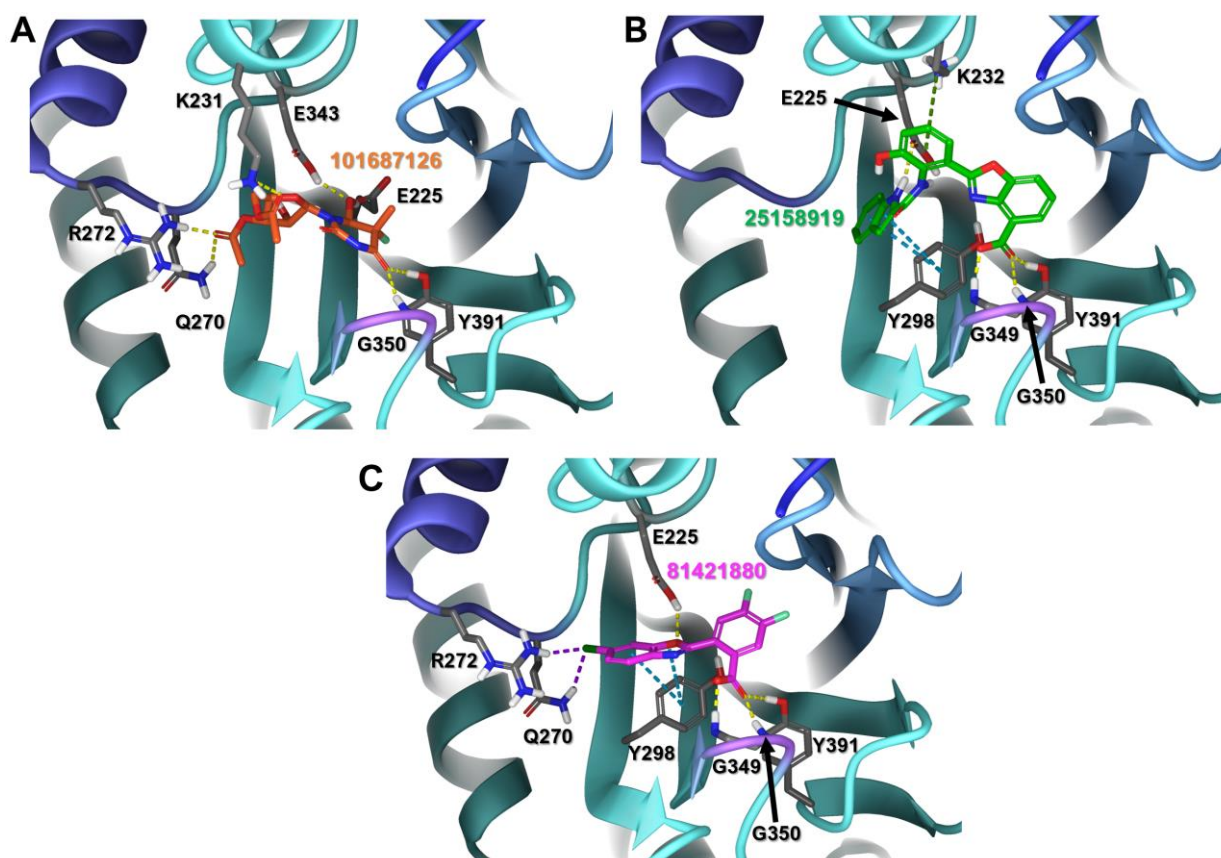


**Figure 4.** HPSE in complex with the best potential inhibitors from each library screening of each library: (A) 101,687,126 (orange); (B) 25,158,919 (green); (C) 81,421,830 (pink). Interactions are shown in dashed lines: H-bond (yellow); halogen bond (purple); pi-pi stacking (blue); pi-cation (green). All the potential HPSE inhibitors are shown in stick representation.

### 3. Materials and Methods

A general overview of the computational workflow is provided in Figure S2.

#### 3.1. Receptor Structure

In this study, a 3D model of the human heparanase enzyme (HPSE) based on a crystal structure that was solved at high resolution (PDB: 5E9C) was used to dock potential heparanase inhibitors. The crystal structure was carefully selected from a comparative analysis of the crystal structures of several heparanases (Table S1). Initial protein optimization of the chosen HPSE 3D structure was carried out using the Protein Preparation Wizard module that is integrated within the Maestro suite software (Schrödinger, LLC, New York, NY, USA, 2020).

#### 3.2. Chemical Database Curation

##### 3.2.1. Previously Reported inhibitors

Known HPSE inhibitors were retrieved from the ChEMBL database [38,39]. A total of 573 known HPSE modulators were considered for the analysis of their interaction with the target molecule HPSE. The DataWarrior software [57] was used to discard chemical structure duplicates as well as for data analysis of reported information along with our computed docking scores.

### 3.2.2. Similarity Libraries

Taking into account structural diversity, binding mode, docking scores, IC<sub>50</sub> values and lack of reported off-targets, compounds ChEMBL2349247, ChEMBL495255, ChEMBL4294823 and ChEMBL2349245 were selected as the most promising hits for further computational studies. These molecules were used as a structural basis to retrieve four independent chemical libraries of structurally similar compounds from *PubChem* [42]. The criteria applied to obtain these chemical libraries, along with the number of compounds they each returned are shown in Table 4.

**Table 4.** Selection criteria of chemical libraries obtained from PubChem.

	Chemical Library 1 (ChEMBL2349245)	Chemical Library 2 (ChEMBL495255)	Chemical Library 3 (ChEMBL2349247)	Chemical Library 4 (ChEMBL4294823)
Tanimoto similarity index	>70%	>80%	>80%	>80%
Molecular Weight (g/mol)	200–600	200–600	200–600	200–600
Rotatable bond count	2–10	2–10	2–10	2–10
Heavy atom count	17–33	17–35	17–35	17–35
xLog(P)	−8–3	3–9	3–9	3–9
No. of compounds returned	4938	9923	34,721	34,721

### 3.2.3. Ligand Preparation

Low-energy three-dimensional conformations of each molecule of the aforementioned chemical databases were obtained using the LigPrep module within the Maestro suite (Schrödinger, LLC, New York, NY, USA, 2020). The Epik software was employed to predict pK<sub>a</sub> values in the 7.0–7.5 pH range and to identify every chemically sensible structure using the Hammett and Taft methodology [58]. All compounds were minimized using the OPLS4 force field implemented in Maestro [59].

## 3.3. Molecular Docking Studies

### 3.3.1. Grid GENERATION

Prior to using the Glide module high-throughput virtual screening (HTVS) and extra precise (XP) docking within the Schrödinger package (Schrödinger, LLC, New York, NY, USA, 2020), docking grids were generated using the receptor grid generation tool within Glide to ensure ligand screening was performed in the appropriate site within HPSE. To ensure a range that covered both HBD-1 and HBD-2, the dimensions of the HPSE grid were set at 26 Å in length along the x, y and z axes and was centered on the co-crystallized ligand.

### 3.3.2. HTVS and XP Docking

HTVS and XP docking calculations were performed using the Virtual Screening Workflow tool and the XP Glide-dock modules integrated within the Schrödinger package [60,61]. Every analyzed structure was explored in the binding site of the HPSE target. Given the nature of the catalytic mechanism of HPSE, the Glu225 residue had to be protonated to ensure a proper ligand–enzyme interaction. Ligand flexibility was considered to explore an arbitrary number of torsional degrees of freedom, in addition to the six spatial degrees of freedom spanned by translational and rotational parameters. Ligand poses thus generated were run through a series of hierarchical filters to evaluate ligand interactions with HPSE. Energy minimization was performed with the OPLS4 force field. The top 10% scoring compounds from the HTVS were selected for further analysis using XP Glide docking. The top 30% of ligands obtained from the XP screening were thoroughly analyzed taking into account docking scores, ligand/receptor interactions, binding mode and previously reported HPSE inhibitory activity.

### 3.3.3. Additional Selection Criteria

In the search for potential novel HPSE inhibitors, we also considered the following criteria to filter and select the most promising hits.

#### In Silico ADME Parameters

A set of physico-chemical properties was calculated using QikProp integrated in Maestro (Schrödinger, LLC, New York, NY, USA). Table 3 shows the QikProp parameters of selected compounds. The 3D LigPrep conformations obtained for each molecule were used as the input in the calculation of QikProp descriptors.

#### PAINS Identification

In order to avoid the presence of potential promiscuous moieties or PAINS (pan-assay interference compounds) [62,63], all the molecules were analyzed using the swissADME webserver [43] to filter-off molecules containing such chemical groups.

## 4. Conclusions

There is mounting evidence showing that the upregulation of HPSE correlates with tumor progression as well as several diseases associated with chronic inflammation, including COVID-19. Consequently, the discovery of molecules that inhibit HPSE is of broad therapeutic interest. However, most currently available HPSE inhibitors bear a very high molecular weight along with an unfavorable druggability profile. In this project we developed a chemoinformatics approach to identify potential novel HPSE inhibitors with optimal drug-like features. The compounds thus identified can be used as lead chemotypes to develop novel therapeutics for the treatment of chronic and infectious diseases associated with chronic inflammation.

Future work will aim to synthesize and test the biological activity of selected potential HPSE inhibitors in an attempt to develop lead compounds. These efforts should advance the design of more effective HPSE inhibitors for the treatment of severe inflammatory pathological processes.

**Supplementary Materials:** The following are available online at <https://www.mdpi.com/article/10.3390/catal12050503/s1>, Figure S1: Heparanase inhibitors; Figure S2: Workflow used in this study for the identification of novel HPSE inhibitors; Table S1: Heparanases 3D structures retrieved from the Protein Data Bank (PDB); Table S2: Docking scores and reported data of known HPSE inhibitors (\*separate spreadsheet); Figure S3: Ligand interaction diagrams of selected hit HPSE inhibitors ChEMBL2349245, ChEMBL495255, ChEMBL2349247 and ChEMBL4294823; Table S3: Data reported for selected potential HPSE inhibitors; Figure S4: Docking studies of HPSE in complex with selected potential HPSE inhibitors; Figure S5: Ligand interaction diagrams of selected potential HPSE inhibitors. References [36,40,44–56,64] are cited in Supplementary Materials.

**Author Contributions:** Conceptualization, A.B. and P.M.; methodology, A.B. and P.M.; validation, A.R., A.B. and P.M.; formal analysis, A.R. and P.M.; investigation, A.R., A.B. and P.M.; data curation, A.R.; writing—original draft preparation, A.R. and P.M.; writing—review and editing, A.B. and V.M.B.-G.; supervision, A.B., V.M.B.-G. and P.M.; funding acquisition, A.B. All authors have read and agreed to the published version of the manuscript.

**Funding:** This research was funded by Ministerio de Economía Industria y Competitividad grant number PID2019-105337RB-C21 and the state agency Spanish national research council (CSIC), Program i-LINK (LINKB20075).

**Data Availability Statement:** Databases used: PubChem and ChEMBL.

**Acknowledgments:** Paula Morales acknowledges the Spanish Ministry of Science and Innovation for her postdoctoral fellow from the Juan de la Cierva Incorporación Programme-MICIU (IJC 2019-042182-I).

**Conflicts of Interest:** The authors declare no conflict of interest.



## References

1. Giannini, G.; Battistuzzi, G.R.S. *Heparanase: From Basic Research to Clinical Applications*; Vlodavsky, I., Sanderson, R.D., Ilan, N., Eds.; Springer: Berlin/Heidelberg, Germany, 2020; pp. 567–598, ISBN 9783030345204.
2. Nasser, N.J. Heparanase involvement in physiology and disease. *Cell. Mol. Life Sci.* **2008**, *65*, 1706–1715. [[CrossRef](#)] [[PubMed](#)]
3. Wu, L.; Viola, C.M.; Brzozowski, A.M.; Davies, G.J. Structural characterization of human heparanase reveals insights into substrate recognition. *Nat. Struct. Mol. Biol.* **2015**, *22*, 1016–1022. [[CrossRef](#)] [[PubMed](#)]
4. Coombe, D.R.; Gandhi, N.S. Heparanase: A Challenging Cancer Drug Target. *Front. Oncol.* **2019**, *9*, 1316. [[CrossRef](#)] [[PubMed](#)]
5. Peterson, S.; Liu, J. Deciphering mode of action of heparanase using structurally defined oligosaccharides. *J. Biol. Chem.* **2012**, *287*, 34836–34843. [[CrossRef](#)]
6. Yu, Y.; Williams, A.; Zhang, X.; Fu, L.; Xia, K.; Xu, Y.; Zhang, F.; Liu, J.; Koffas, M.; Linhardt, R.J. Specificity and action pattern of heparanase Bp, a  $\beta$ -glucuronidase from *Burkholderia pseudomallei*. *Glycobiology* **2019**, *29*, 572–581. [[CrossRef](#)]
7. Levy-Adam, F.; Abboud-Jarrous, G.; Guerrini, M.; Beccati, D.; Vlodavsky, I.; Ilan, N. Identification and characterization of heparin/heparan sulfate binding domains of the endoglycosidase heparanase. *J. Biol. Chem.* **2005**, *280*, 20457–20466. [[CrossRef](#)]
8. Kudchadkar, R.; Gonzalez, R.; Lewis, K.D. PI-88: A novel inhibitor of angiogenesis. *Expert Opin. Investig. Drugs* **2008**, *17*, 1769–1776. [[CrossRef](#)]
9. Liang, X.-J.; Yuan, L.; Hu, J.; Yu, H.-H.; Li, T.; Lin, S.-F.; Tang, S.-B. Phosphomannopentaose sulfate (PI-88) suppresses angiogenesis by downregulating heparanase and vascular endothelial growth factor in an oxygen-induced retinal neovascularization animal model. *Mol. Vis.* **2012**, *18*, 1649–1657.
10. Zhou, H.; Roy, S.; Cochran, E.; Zouaoui, R.; Chu, C.L.; Duffner, J.; Zhao, G.; Smith, S.; Galcheva-Gargova, Z.; Karlgren, J.; et al. M402, a Novel Heparan Sulfate Mimetic, Targets Multiple Pathways Implicated in Tumor Progression and Metastasis. *PLoS ONE* **2011**, *6*, e21106. [[CrossRef](#)]
11. Macdonald, A.; Priess, M.; Curran, J.; Guess, J.; Farutin, V.; Oosterom, I.; Lin Chu, C.; Cochran, E.; Zhang, L.; Getchell, K.; et al. Small Molecule Therapeutics Necuparanib, a Multitargeting Heparan Sulfate Mimetic, Targets Tumor and Stromal Compartments in Pancreatic Cancer. *Mol. Cancer Ther.* **2019**, *18*, 245–256. [[CrossRef](#)]
12. O'Reilly, E.M.; Roach, J.; Miller, P.; Yu, K.H.; Tjan, C.; Rosano, M.; Krause, S.; Avery, W.; Wolf, J.; Flaherty, K.; et al. Safety, Pharmacokinetics, Pharmacodynamics, and Antitumor Activity of Necuparanib Combined with Nab-Paclitaxel and Gemcitabine in Patients with Metastatic Pancreatic Cancer: Phase I Results. *Oncologist* **2017**, *22*, 1429. [[CrossRef](#)] [[PubMed](#)]
13. Barbieri, P.; Paoletti, D.; Giannini, G.; Sanderson, R.D.; Nosedà, A. Roneparstat and Heparanase Inhibition: A New Tool for Cancer Treatment. *J. Pharmacol. Clin. Toxicol.* **2017**, *5*, 1071.
14. Pala, D.; Rivara, S.; Mor, M.; Milazzo, F.M.; Roscilli, G.; Pavoni, E.; Giannini, G. Kinetic analysis and molecular modeling of the inhibition mechanism of roneparstat (SST0001) on human heparanase. *Glycobiology* **2016**, *26*, 640–654. [[CrossRef](#)]
15. Cassinelli, G.; Favini, E.; Bo, L.D.; Tortoreto, M.; De Maglie, M.; Dagrada, G.; Pilotti, S.; Zunino, F.; Zaffaroni, N.; Lanzi, C. Antitumor efficacy of the heparan sulfate mimic roneparstat (SST0001) against sarcoma models involves multi-target inhibition of receptor tyrosine kinases. *Oncotarget* **2016**, *7*, 47848–47863. [[CrossRef](#)]
16. Ritchie, J.P.; Ramani, V.C.; Ren, Y.; Naggi, A.; Torri, G.; Casu, B.; Penco, S.; Pisano, C.; Carminati, P.; Tortoreto, M.; et al. SST0001, a chemically modified heparin, inhibits myeloma growth and angiogenesis via disruption of the heparanase/syndecan-1 axis. *Clin. Cancer Res.* **2011**, *17*, 1382–1393. [[CrossRef](#)]
17. Rossini, A.; Zunino, F.; Ruggiero, G.; De Cesare, M.; Cominetti, D.; Tortoreto, M.; Lanzi, C.; Cassinelli, G.; Zappasodi, R.; Tripodo, C.; et al. Microenvironment modulation and enhancement of antilymphoma therapy by the heparanase inhibitor roneparstat. *Hematol. Oncol.* **2018**, *36*, 360–362. [[CrossRef](#)]
18. Galli, M.; Chatterjee, M.; Grasso, M.; Specchia, G.; Magen, H.; Einsele, H.; Celeghini, I.; Barbieri, P.; Paoletti, D.; Pace, S.; et al. Phase I study of the heparanase inhibitor roneparstat: An innovative approach for multiple myeloma therapy. *Haematologica* **2018**, *103*, e469–e472. [[CrossRef](#)]
19. Dredge, K.; Hammond, E.; Davis, K.; Li, C.P.; Liu, L.; Johnstone, K.; Handley, P.; Wimmer, N.; Gonda, T.J.; Gautam, A.; et al. The PG500 series: Novel heparan sulfate mimetics as potent angiogenesis and heparanase inhibitors for cancer therapy. *Investig. New Drugs* **2010**, *28*, 276–283. [[CrossRef](#)]
20. Ferro, V.; Liu, L.; Johnstone, K.D.; Wimmer, N.; Karoli, T.; Handley, P.; Rowley, J.; Dredge, K.; Li, C.P.; Hammond, E.; et al. Discovery of PG545: A highly potent and simultaneous inhibitor of angiogenesis, tumor growth, and metastasis. *J. Med. Chem.* **2012**, *55*, 3804–3813. [[CrossRef](#)]
21. Weissmann, M.; Bhattacharya, U.; Feld, S.; Hammond, E.; Ilan, N.; Vlodavsky, I. The heparanase inhibitor PG545 is a potent anti-lymphoma drug: Mode of action. *Matrix Biol.* **2019**, *77*, 58–72. [[CrossRef](#)]
22. Hammond, E.; Handley, P.; Dredge, K.; Bytheway, I. Mechanisms of heparanase inhibition by the heparan sulfate mimetic PG545 and three structural analogues. *FEBS Open Bio* **2013**, *3*, 346–351. [[CrossRef](#)] [[PubMed](#)]
23. Loka, R.S.; Sletten, E.T.; Barash, U.; Vlodavsky, I.; Nguyen, H.M. Specific Inhibition of Heparanase by a Glycopolymer with Well-Defined Sulfation Pattern Prevents Breast Cancer Metastasis in Mice. *ACS Appl. Mater. Interfaces* **2019**, *11*, 244–254. [[CrossRef](#)] [[PubMed](#)]
24. Madia, V.N.; Messore, A.; Pescatori, L.; Saccoliti, F.; Tudino, V.; De Leo, A.; Bortolami, M.; Scipione, L.; Costi, R.; Rivara, S.; et al. Novel Benzazole Derivatives Endowed with Potent Antiheparanase Activity. *J. Med. Chem.* **2018**, *61*, 6918–6936. [[CrossRef](#)]

25. Seto, H.; Furuya, K.; Takahashi, S.; Takahashi, M.; Tanzawa, K. Trachyspic Acid, a New Metabolite Produced by *Talaromyces trachyspermus*, that Inhibits Tumor Cell Heparanase: Taxonomy of the Producing Strain, Fermentation, Isolation, Structural Elucidation, and Biological Activity. *J. Antibiot.* **1995**, *48*, 357–362.
26. Wang, P.; Zhang, Z.; Yu, B. Total synthesis of CRM646-A and -B, two fungal glucuronides with potent heparinase inhibition activities. *J. Org. Chem.* **2005**, *70*, 8884–8889. [[CrossRef](#)] [[PubMed](#)]
27. Yan, L.; Yan, K.; Kun, W.; Xu, L.; Ma, Q.; Tang, Y.; Jiao, W.; Gu, G.; Fan, Y.; Xu, Z. Berberine inhibits the migration and invasion of T24 bladder cancer cells via reducing the expression of heparanase. *Tumor Biol.* **2013**, *34*, 215–221. [[CrossRef](#)] [[PubMed](#)]
28. Zhang, Y.; Sun, X.; Nan, N.; Cao, K.-X.; Ma, C.; Yang, G.-W.; Yu, M.-W.; Yang, L.; Li, J.-P.; Wang, X.-M.; et al. Elemene inhibits the migration and invasion of 4T1 murine breast cancer cells via heparanase. *Mol. Med. Rep.* **2017**, *16*, 794–800. [[CrossRef](#)]
29. Pangestuti, R.; Kim, S.K. Biological activities of Carrageenan. In *Advances in Food and Nutrition Research*; Academic Press Inc.: Cambridge, MA, USA, 2014; Volume 72, pp. 113–124.
30. Poupard, N.; Groult, H.; Bodin, J.; Bridiau, N.; Bordenave-Juchereau, S.; Sannier, F.; Piot, J.M.; Fruitier-Arnaudin, I.; Maugard, T. Production of heparin and  $\lambda$ -carrageenan anti-heparanase derivatives using a combination of physicochemical depolymerization and glycol splitting. *Carbohydr. Polym.* **2017**, *166*, 156–165. [[CrossRef](#)]
31. Courtney, S.M.; Hay, P.A.; Buck, R.T.; Colville, C.S.; Porter, D.W.; Scopes, D.I.C.; Pollard, F.C.; Page, M.J.; Bennett, J.M.; Hircock, M.L.; et al. 2,3-Dihydro-1,3-dioxo-1H-isoindole-5-carboxylic acid derivatives: A novel class of small molecule heparanase inhibitors. *Bioorg. Med. Chem. Lett.* **2004**, *14*, 3269–3273. [[CrossRef](#)]
32. Nakajima, M.; DeChavigny, A.; Johnson, C.E.; Hamada, J.I.; Stein, C.A.; Nicolson, G.L. Suramin: A potent inhibitor of melanoma heparanase and invasion. *J. Biol. Chem.* **1991**, *266*, 9661–9666. [[CrossRef](#)]
33. Ayal-Hershkovitz, M.; Miron, D.; Levy, O. Benz-1,3-azole Derivatives and Their Uses as Heparanase Inhibitors. WO2002060374, 8 August 2002.
34. Courtney, S.M.; Hay, P.A.; Buck, R.T.; Colville, C.S.; Phillips, D.J.; Scopes, D.I.C.; Pollard, F.C.; Page, M.J.; Bennett, J.M.; Hircock, M.L.; et al. Furanyl-1,3-thiazol-2-yl and benzoxazol-5-yl acetic acid derivatives: Novel classes of heparanase inhibitor. *Bioorg. Med. Chem. Lett.* **2005**, *15*, 2295–2299. [[CrossRef](#)]
35. Baburajeev, C.P.; Mohan, C.D.; Rangappa, S.; Mason, D.J.; Fuchs, J.E.; Bender, A.; Barash, U.; Vlodaysky, I.; Basappa; Rangappa, K.S. Identification of Novel Class of Triazolo-Thiadiazoles as Potent Inhibitors of Human Heparanase and their Anticancer Activity. *BMC Cancer* **2017**, *17*, 235. [[CrossRef](#)]
36. Gozalbes, R.; Mosulén, S.; Orti, L.; Rodríguez-Díaz, J.; Carbajo, R.J.; Melnyk, P.; Pineda-Lucena, A. Hit identification of novel heparanase inhibitors by structure- and ligand-based approaches. *Bioorg. Med. Chem.* **2013**, *21*, 1944–1951. [[CrossRef](#)]
37. Masola, V.; Bellin, G.; Gambaro, G.; Onisto, M. cells Heparanase: A Multitasking Protein Involved in Extracellular Matrix (ECM) Remodeling and Intracellular Events. *Cells* **2018**, *7*, 236. [[CrossRef](#)]
38. Mendez, D.; Gaulton, A.; Bento, A.P.; Chambers, J.; De Veij, M.; Félix, E.; Magariños, M.P.; Mosquera, J.F.; Mutowo, P.; Nowotka, M.; et al. ChEMBL: Towards direct deposition of bioassay data. *Nucleic Acids Res.* **2019**, *47*, D930–D940. [[CrossRef](#)]
39. Davies, M.; Nowotka, M.; Papadatos, G.; Dedman, N.; Gaulton, A.; Atkinson, F.; Bellis, L.; Overington, J.P. ChEMBL web services: Streamlining access to drug discovery data and utilities. *Nucleic Acids Res.* **2015**, *43*, W612–W620. [[CrossRef](#)]
40. Takahashi, H.; Matsumoto, H.; Smirkin, A.; Itai, T.; Nishimura, Y.; Tanaka, J. Involvement of heparanase in migration of microglial cells. *Biochim. Biophys. Acta—Gen. Subj.* **2008**, *1780*, 709–715. [[CrossRef](#)]
41. Messori, A.; Madia, V.N.; Pescatori, L.; Saccoliti, F.; Tudino, V.; De Leo, A.; Bortolami, M.; De Vita, D.; Scipione, L.; Pepi, F.; et al. Novel Symmetrical Benzazolyl Derivatives Endowed with Potent Anti-Heparanase Activity. *J. Med. Chem.* **2018**, *61*, 10834–10859. [[CrossRef](#)]
42. Kim, S.; Thiessen, P.A.; Bolton, E.E.; Chen, J.; Fu, G.; Gindulyte, A.; Han, L.; He, J.; He, S.; Shoemaker, B.A.; et al. PubChem substance and compound databases. *Nucleic Acids Res.* **2016**, *44*, D1202–D1213. [[CrossRef](#)]
43. Daina, A.; Michielin, O.; Zoete, V. SwissADME: A free web tool to evaluate pharmacokinetics, drug-likeness and medicinal chemistry friendliness of small molecules. *Sci. Rep.* **2017**, *7*, 42717. [[CrossRef](#)]
44. 1-(3-O,5-O-Diacetyl-beta-D-ribofuranosyl)-5-methyl-5-fluoro-6-hydroxydihydropyrimidine-2,4(1H,3H)-dione | C<sub>14</sub>H<sub>19</sub>FN<sub>2</sub>O<sub>9</sub>—PubChem. Available online: <https://pubchem.ncbi.nlm.nih.gov/compound/101687126> (accessed on 10 March 2022).
45. 2-[(3-Ethoxycarbonylpiperidine-1-carbonyl)amino]-3-hydroxybutanoic Acid | C<sub>13</sub>H<sub>22</sub>N<sub>2</sub>O<sub>6</sub>—PubChem. Available online: <https://pubchem.ncbi.nlm.nih.gov/compound/61187649> (accessed on 10 March 2022).
46. (2R)-4-Hydroxy-2-[[3-(trifluoromethyl)piperidine-1-carbonyl]amino]butanoic acid | C<sub>11</sub>H<sub>17</sub>F<sub>3</sub>N<sub>2</sub>O<sub>4</sub>—PubChem. Available online: <https://pubchem.ncbi.nlm.nih.gov/compound/107828179> (accessed on 10 March 2022).
47. 4-[Methyl-[(1-methyl-6-oxopiperidin-3-yl)carbamoyl]amino]oxolane-3-carboxylic acid | C<sub>13</sub>H<sub>21</sub>N<sub>3</sub>O<sub>5</sub>—PubChem. Available online: <https://pubchem.ncbi.nlm.nih.gov/compound/66265156> (accessed on 10 March 2022).
48. Tipparaju, S.K.; Joyasawal, S.; Pieroni, M. In Pursuit of Natural Product Leads: Synthesis and Biological Evaluation of 2-[3-hydroxy-2-[(3-hydroxypyridine-2-carbonyl)amino]phenyl]benzoxazole-4-carboxylic acid (A-33853) and Its Analogues: Discovery of N-(2-Benzoxazol-2-ylphenyl)benzamides as Novel Antileishmanial Chemotypes. *J. Med. Chem.* **2008**, *51*, 7344–7347.
49. 3-Phenanthro[9,10-d][1,3]oxazol-2-ylpropanoic acid | C<sub>18</sub>H<sub>13</sub>NO<sub>3</sub>—PubChem. Available online: <https://pubchem.ncbi.nlm.nih.gov/compound/23794729> (accessed on 10 March 2022).
50. 2-(6-Fluoro-1,3-benzoxazol-2-yl)-3,6-dimethylbenzoic acid | C<sub>16</sub>H<sub>12</sub>FNO<sub>3</sub>—PubChem. Available online: <https://pubchem.ncbi.nlm.nih.gov/compound/103430682> (accessed on 10 March 2022).

51. 2-[[3-(1,3-Benzoxazol-2-yl)propanoylamino]methyl]-3-(3-methylphenyl)propanoic acid | C<sub>21</sub>H<sub>22</sub>N<sub>2</sub>O<sub>4</sub>—PubChem. Available online: <https://pubchem.ncbi.nlm.nih.gov/compound/119243009> (accessed on 10 March 2022).
52. 2-(6-Chloro-1,3-benzoxazol-2-yl)-4,5-difluorobenzoic acid | C<sub>14</sub>H<sub>6</sub>ClF<sub>2</sub>NO<sub>3</sub>—PubChem. Available online: <https://pubchem.ncbi.nlm.nih.gov/compound/81421830> (accessed on 10 March 2022).
53. Stephen, I.; Courtney, M.; Hay, P.A.; Ian, D.; Scopes, C.; Gb, O. Phtalamide Carboxylic Acid Derivatives. US-7138425-B2, 21 November 2006.
54. 2'-(Benzo[d]oxazol-2-yl)-[1,1'-biphenyl]-2-carboxylate | C<sub>20</sub>H<sub>12</sub>NO<sub>3</sub>—PubChem. Available online: <https://pubchem.ncbi.nlm.nih.gov/compound/155906206> (accessed on 10 March 2022).
55. 5-[2-(1,3-Benzoxazol-2-yl)sulfanyl]propanoylamino]-2-chlorobenzoic acid | C<sub>17</sub>H<sub>13</sub>ClN<sub>2</sub>O<sub>4</sub>S—PubChem. Available online: <https://pubchem.ncbi.nlm.nih.gov/compound/23886486> (accessed on 10 March 2022).
56. 5-[3-(1,3-Benzoxazol-2-yl)anilino]-5-oxopentanoate | C<sub>18</sub>H<sub>15</sub>N<sub>2</sub>O<sub>4</sub>—PubChem. Available online: <https://pubchem.ncbi.nlm.nih.gov/compound/6968873> (accessed on 10 March 2022).
57. Sander, T.; Freyss, J.; Von Korff, M.; Rufener, C. DataWarrior: An open-source program for chemistry aware data visualization and analysis. *J. Chem. Inf. Model.* **2015**, *55*, 460–473. [[CrossRef](#)]
58. Greenwood, J.R.; Calkins, D.; Sullivan, A.P.; Shelley, J.C. Towards the comprehensive, rapid, and accurate prediction of the favorable tautomeric states of drug-like molecules in aqueous solution. *J. Comput. Aided. Mol. Des.* **2010**, *24*, 591–604. [[CrossRef](#)]
59. Lu, C.; Wu, C.; Ghoreishi, D.; Chen, W.; Wang, L.; Damm, W.; Ross, G.A.; Dahlgren, M.K.; Russell, E.; Von Bargen, C.D.; et al. OPLS4: Improving force field accuracy on challenging regimes of chemical space. *J. Chem. Theory Comput.* **2021**, *17*, 4291–4300. [[CrossRef](#)]
60. Warren, G.L.; Andrews, C.W.; Capelli, A.M.; Clarke, B.; LaLonde, J.; Lambert, M.H.; Lindvall, M.; Nevins, N.; Semus, S.F.; Senger, S.; et al. A critical assessment of docking programs and scoring functions. *J. Med. Chem.* **2006**, *49*, 5912–5931. [[CrossRef](#)]
61. Friesner, R.A.; Murphy, R.B.; Repasky, M.P.; Frye, L.L.; Greenwood, J.R.; Halgren, T.A.; Sanschagrin, P.C.; Mainz, D.T. Extra precision glide: Docking and scoring incorporating a model of hydrophobic enclosure for protein-ligand complexes. *J. Med. Chem.* **2006**, *49*, 6177–6196. [[CrossRef](#)]
62. Baell, J.B.; Holloway, G.A. New substructure filters for removal of pan assay interference compounds (PAINS) from screening libraries and for their exclusion in bioassays. *J. Med. Chem.* **2010**, *53*, 2719–2740. [[CrossRef](#)]
63. Capuzzi, S.J.; Muratov, E.N.; Tropsha, A. Phantom PAINS: Problems with the Utility of Alerts for Pan-Assay in terference Compounds. *J. Chem. Inf. Model.* **2017**, *57*, 417–427. [[CrossRef](#)]
64. 4-Hydroxy-1-(4,4,4-trifluorobutylcarbamoyl)pyrrolidine-2-carboxylic acid | C<sub>10</sub>H<sub>15</sub>F<sub>3</sub>N<sub>2</sub>O<sub>4</sub>—PubChem. Available online: <https://pubchem.ncbi.nlm.nih.gov/compound/113327907> (accessed on 10 March 2022).